# The baseline intracluster entropy profile from gravitational structure formation

G. Mark Voit[1]⋆, Scott T. Kay[2], and Greg L. Bryan[3]

[1] *Department of Physics and Astronomy, Michigan State University, East Lansing, MI 48824, USA*
[2] *Physics Department, University of Oxford, Keble Road, Oxford OX1 3RH, UK*
[3] *Department of Astronomy, Columbia University, New York, NY 10027, USA*

**ABSTRACT**
The radial entropy profile of the hot gas in clusters of galaxies tends to follow a power law in radius outside of the cluster core. Here we present a simple formula giving both the normalization and slope for the power-law entropy profiles of clusters that form in the absence of non-gravitational processes such as radiative cooling and subsequent feedback. It is based on seventy-one clusters drawn from four separate cosmological simulations, two using smoothed-particle hydrodynamics (SPH) and two using adaptive-mesh refinement (AMR), and can be used as a baseline for assessing the impact of non-gravitational processes on the intracluster medium outside of cluster cores. All the simulations produce clusters with self-similar structure in which the normalization of the entropy profile scales linearly with cluster temperature, and these profiles are in excellent agreement outside of $0.2r_{200}$. Because the observed entropy profiles of clusters do not scale linearly with temperature, our models confirm that non-gravitational processes are necessary to break the self-similarity seen in the simulations. However, the core entropy levels found by the two codes used here significantly differ, with the AMR code producing nearly twice as much entropy at the centre of a cluster.

**Key words:** cosmology: theory — galaxies: clusters: general — galaxies: evolution — intergalactic medium — X-rays: galaxies: clusters

## 1 INTRODUCTION

Purely gravitational structure formation ought to produce clusters of galaxies with nearly self-similar structure, whose X-ray luminosity $L_{\rm X}$ scales with temperature $T_{\rm X}$ as $L_{\rm X} \propto T_{\rm X}^2$ (Kaiser 1986). Clusters created in hydrodynamical simulations with cosmological initial conditions indeed follow this scaling relation (e.g., Navarro et al. 1995; Eke et al. 1998), but observed clusters do not. Instead they follow a relation closer to $L_{\rm X} \propto T_{\rm X}^{2.8}$ (Edge & Stewart 1991; David et al. 1995; Markevitch 1998; Allen & Fabian 1998; Arnaud & Evrard 1999). Somehow the non-gravitational cooling and heating processes associated with galaxy formation intervene to break the expected self-similarity, with consequences that are more severe in low-temperature clusters than in high-temperature clusters (Kaiser 1991; Evrard & Henry 1991, see Voit 2005 for a recent review).

The scaling behavior of the $L_{\rm X}$-$T_{\rm X}$ relation can largely be understood in terms of radiative cooling and the feedback it triggers (Voit & Bryan 2001). Gas that can cool within a Hubble time must either condense, forming stars or cold baryonic clouds, or it must be reheated somehow, probably by supernovae or AGN activity triggered by the condensing gas. Because $\sim 85\%$ of the baryons associated with a massive cluster appear to be in the hot intracluster medium (ICM), a certain amount of supernova or AGN feedback seems necessary to prevent too many of the baryons from condensing during the formation of a cluster's galaxies (White & Frenk 1991; Balogh et al. 2001). However, the $L_{\rm X}$-$T_{\rm X}$ relation itself is relatively insensitive to the total amount of feedback energy, as long as the energy input into the reheated gas is sufficient to keep it from cooling again (Borgani et al. 2002; Kay et al. 2003; Tornatore et al. 2003; Valdarnini 2003). Thus, one needs to look beyond the $L_{\rm X}$-$T_{\rm X}$ relation in order to assess the thermodynamic impact of supernovae and AGNs on the state of the ICM.

One good place to look for more information is in the spatially-resolved entropy profiles of clusters and groups, which preserve a record of the cooling and heating processes responsible for similarity breaking in clusters (Voit et al. 2002; Voit et al. 2003; Kay 2004; Kay et al. 2004). Spe-

---

⋆ E-mail: voit@pa.msu.edu (GMV); skay@astro.ox.ac.uk (STK); gbryan@astro.columbia.edu (GLB)

cific entropy, represented in this paper by the quantity $K = T n_e^{-2/3}$, where $n_e$ is the electron density, is more closely tied to the thermodynamic history of a cluster than is temperature, because the thermal energy of heated gas can be converted into gravitational potential energy as the heated gas expands in the confining potential well.[1] Under certain circumstances, a large amount of energy input produces only a small rise in the luminosity-weighted temperature $T_X$ (e.g., Voit et al. 2002). The specific entropy of the ICM, on the other hand, always rises when heat energy is introduced and always falls when radiative cooling carries heat energy away.

The entropy profiles of clusters and groups can now be measured out to a significant fraction of the scale radius $r_{200}$, within which the mean mass density is 200 times the critical density. Those measurements show that entropy levels in the cores of clusters, where the $L_X$-$T_X$ relation is determined, scale as $K_{0.1} \equiv K(0.1 r_{200}) \propto T_X^{2/3}$ (Ponman et al. 2003), as expected if radiative cooling and associated feedback govern the core entropy level (Voit & Ponman 2003). More surprisingly, entropy measurements at larger cluster radii are hinting that this scaling relation applies to the entire entropy profile. Deep *XMM-Newton* observations of five clusters whose temperatures span a range of ∼3.5 show that the scaled profile $T_X^{-2/3} K(r/r_{200})$ is independent of cluster temperature (Pratt & Arnaud 2003; Pratt & Arnaud 2005). Likewise, an analysis of lower-quality data on a larger number of clusters also suggests that $K(r/r_{200}) \propto T_X^{2/3}$ at the scale radius $r_{500}$, within which the mean matter density is 500 times the critical density (Ponman et al. 2003).

Rather than totally breaking the self-similarity of clusters, galaxy formation appears to alter the power-law scaling of $K(r/r_{200})$ with $T_X$ without appreciably changing the overall shape of the entropy profile. Exactly how heating and cooling would conspire to produce such a shape-preserving shift in the normalization of an intracluster entropy profile is unknown. One possibility involves smoothing of the intergalactic medium by supernovae or AGN energy input prior to accretion, which lowers the mass-weighted mean density $\bar{\rho}_{acc}$ of the infalling gas. Because the amount of entropy generated in that gas when it passes through accretion shocks of velocity $v_{acc}$ is $K_{acc} \sim v_{acc}^2 / \bar{\rho}_{acc}^{2/3}$, smoothing of gas that would otherwise be bound to accreting subhalos boosts the post-accretion entropy level of the ICM (Voit et al. 2003; Ponman et al. 2003; Borgani et al. 2005). Another possibility, illustrated in simulations by Kay (2004), involves uncompensated cooling, which allows high-entropy gas to sink to smaller radii as the core gas condenses, but pure cooling does not appear to reproduce the $K \propto T_X^{2/3}$ relation at $r_{500}$.

A proper analysis of the observations to determine the true source of the entropy boost requires knowing what the baseline entropy profile of a cluster would be like in the absence of galaxy formation. To that end, this paper compares the results of four different hydrodynamical simulations of purely gravitational cluster formation with the aim of deriving a simple analytical formula for that baseline self-similar entropy profile. The hydrodynamical computations in the simulations employ entirely different numerical algorithms: some use smoothed-particle hydrodynamics (SPH) while the others use adaptive-mesh refinement (AMR). Thus, to the extent that these two techniques produce convergent results, our comparison provides a reliable baseline profile with which to interpret the observations. Our comparison shows that the codes agree and are presumably reliable outside the cores of clusters, where entropy levels are relatively high, but disagree inside the cores, where entropy levels are lower. This discrepancy is not yet understood and may result from differences in how the codes treat small-scale shocks and mixing processes.

While the cosmological parameters used to specify the initial conditions in the simulations are similar—ΛCDM, with matter density $\Omega_M \approx 0.3$, dark-energy density $\Omega_\Lambda \approx 0.7$, baryon density $\Omega_b \approx 0.04$, Hubble constant[2] $h \approx 0.7$ and power-spectrum normalization $\sigma_8 \approx 0.9$—the initial conditions themselves are not identical. The simulations do not model the evolution of the same field of density perturbations. Instead, we compare results for many different clusters within representative but not identical volumes of the universe, as modeled by each code.

The paper proceeds as follows. Section 2 establishes a non-dimensional framework for comparing the entropy profiles of clusters having different masses then describes the two codes we use and presents results from each code. In each case we determine the median dimensionless entropy profile and the scatter about the median. Knowing the variance in entropy owing to the non-steady nature of merging should help observers establish whether additional variance generated by the stochasticity of non-gravitational processes is needed to explain the observations. Section 3 compares the results from the two codes and provides a simple analytical form for the baseline entropy profile outside the cluster core that adequately represents the results of both simulations. Because the entropy profiles determined with the two codes disagree somewhat in the cluster core, the formula is valid only for $0.2 \stackrel{<}{\sim} r/r_{200} \stackrel{<}{\sim} 1.0$. Section 4 summarizes our results.

## 2 SIMULATIONS OF NON-RADIATIVE CLUSTERS

Clusters that form without radiating away any of their thermal energy are unphysical, but they constitute a useful baseline against which to measure the effects of radiative cooling and non-gravitational heating (e.g., Voit et al. 2002; Frenk et al. 1999). In spite of the obvious fact that accretion shocks generate an enormous amount of entropy during cluster formation. Such clusters are sometimes called "adiabatic" clusters in the literature on this subject. Because we prefer to reserve the term "adiabatic" for isentropic processes that do not involve shock heating, we will refer to these clusters as "non-radiative" clusters (as in Muanwong et al. 2001).

This section examines two populations of non-radiative clusters generated using both SPH and AMR techniques. The properties of these simulated clusters are most easily compared if we scale away the dependence of dimensional quantities on halo mass, a procedure that would lead to

---

[1] The classical thermodynamic entropy per particle is $s = \ln K^{3/2} + \text{const.}$ in an ideal monoatomic gas.

[2] We define $h \equiv H_0 / (100 \, \mathrm{km \, s^{-1} \, Mpc^{-1}})$.

identical temperature, density, and entropy profiles for each cluster if clusters were precisely self-similar. Thus, we begin by outlining the scaling behavior expected in the self-similar case and then remove all the mass-dependent factors when analyzing the clusters from each simulation. These simulated clusters are not precisely self-similar, in that we typically find a $\sim$20% scatter in entropy at a given scale radius outside $0.1r_{200}$ and a somewhat larger variance inside this radius. However, we find no systematic trends in the scaled entropy with cluster mass; in other words, we find $K(r/r_{200}) \propto T_{\rm X}$ to within $\sim$20% across the entire mass range of adequately resolved clusters. Thus, our models do not support the suggestion of Valageas et al. (2003) that shock heating associated with large-scale structure formation alters the $L_{\rm X}$-$T_{\rm X}$ relation by preferentially elevating the entropy levels in groups. All of the gravitationally-driven entropy production that happens on large scales is well resolved in the simulations, and the simulated clusters turn out to be self-similar over almost two orders of magnitude in mass.

## 2.1 Entropy Scaling Laws

The temperature of a self-similar cluster depends primarily on the mass $M_{200}$ within the radius $r_{200}$, motivating us to define the characteristic temperature scale

$$T_{200} \equiv \frac{GM_{200}\mu m_{\rm p}}{2r_{200}} \quad . \tag{1}$$

Here and throughout the paper we write the temperature in energy units, implicitly absorbing Boltzmann's constant into $T$ because observed X-ray temperatures are so often quoted in units of keV. Simulations of non-radiative clusters generally find that $T_{\rm X} \approx T_{200}$ with a scatter of $\sim$10% (Voit 2005) that apparently depends on the effective resolution of a simulation and the numerical techniques it employs.

The natural entropy scale in the ICM of a non-radiative cluster is therefore $K_{200} \equiv T_{200}\bar{n}_e^{-2/3}$, where $\bar{n}_e$ equals $200\Omega_{\rm M}^{-1}$ times the mean electron density of the universe, which would be the mean electron density inside $r_{200}$ if the electron to dark-matter ratio remained constant. In a $\Lambda$CDM cosmology with a baryon density $\Omega_{\rm b} = 0.022h^{-2}$ one finds $\bar{n}_e = (1.45 \times 10^{-4}\,{\rm cm}^{-3})(\Omega_{\rm M}/0.3)(1+z)^3$, giving

$$\begin{aligned} K_{200} &= 362\,{\rm keV\,cm^2}\,\frac{T_{\rm X}}{1\,{\rm keV}}\,\left(\frac{T_{200}}{T_{\rm X}}\right) \\ &\times \left[\frac{H(z)}{H_0}\right]^{-4/3}\left(\frac{\Omega_{\rm M}}{0.3}\right)^{-4/3} \quad, \end{aligned} \tag{2}$$

where $\Omega_{\rm M}$ is the current value of the matter-density parameter. Writing $K_{200}$ in this way makes explicit the fact that the observed temperature of a cluster is not necessarily a reliable guide to the underlying value of $K_{200}$. If the ICM of a real cluster is either hotter or cooler than $T_{200}$, the characteristic temperature of its halo, then one must apply the correction factor $T_{200}/T_{\rm X}$ when computing the value of $K_{200}$.

Radiative cooling introduces another entropy scale into the ICM that does not enter into the comparison of simulated clusters presented here but may be tied to the observed $K \propto T_{\rm X}^{2/3}$ scaling in real clusters. Gas of temperature $T$ emitting pure thermal bremsstrahlung radiation radiates an energy equivalent to its thermal energy in a time period $t$ if its specific entropy is
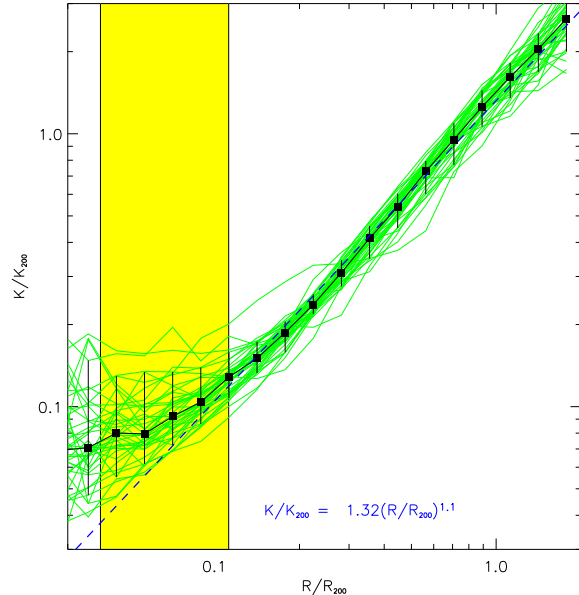


**Figure 1.** Dimensionless entropy $K/K_{200}$ as a function of scale radius $r/r_{200}$ for 40 clusters simulated with the SPH code GADGET. Black squares show the median profile, and the dashed line illustrates the power-law relation $K/K_{200} = 1.32(r/r_{200})^{1.1}$. Most of the entropy profiles shown lie close to this relation in the radial range $0.1 \overset{<}{\sim} r/r_{200} \overset{<}{\sim} 1.0$. At smaller radii, the entropy profiles generally flatten, and their dispersion increases. The shaded box shows the range of radii over which the gravity begins to depart from a precise inverse square law because of gravitational softening. Even though the point at which the entropy profiles begin to flatten coincides with the outer edge of this box, we suspect that the flattening is real because the better-resolved, higher-mass clusters show the same amount of flattening as the lower-mass clusters when scaled relative to $r_{200}$.

$$K_c \approx 81\,{\rm keV\,cm^2}\,\left(\frac{T}{1\,{\rm keV}}\right)^{2/3}\left(\frac{t}{14\,{\rm Gyr}}\right)^{2/3} \quad . \tag{3}$$

Because this entropy threshold for cooling is quite similar to the observed core entropies of many clusters, it seems a quite natural explanation for the $K_{0.1} \propto T_{\rm X}^{2/3}$ scaling found in cluster cores (Voit & Ponman 2003). However, it is less clear why $K \propto T_{\rm X}^{2/3}$ should hold when $K \gg K_c$.

## 2.2 SPH Simulations

The first set of simulated non-radiative clusters we will consider was produced by the entropy-conserving version of the smoothed-particle hydrodynamics code GADGET (Springel et al. 2001; Springel & Hernquist 2002) with $\Omega_{\rm M} = 0.3$, $\Omega_\Lambda = 0.7$, $\Omega_{\rm b} = 0.045$, $h = 0.7$, and $\sigma_8 = 0.9$. Most of this set comes from the non-radiative simulation described in Kay (2004), from which we take the thirty most massive clusters, ranging from $2.1 \times 10^{13}\,h^{-1}\,M_\odot$ to $7.5 \times 10^{14}\,h^{-1}\,M_\odot$. These clusters were modeled within a box of comoving length $60\,h^{-1}$ Mpc using an equivalent Plummer softening length of $20\,h^{-1}$ kpc in comoving coordinates. To supplement the high-mass end of the set, we also include the ten high-mass clusters simulated by Kay et al. (2004), using the same code and the same cosmological parameters. These
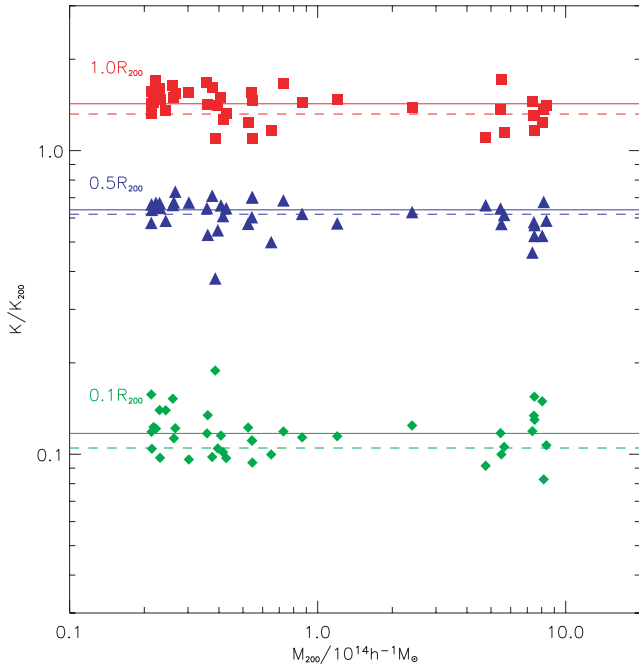
**Figure 2.** Dimensionless entropy $K/K_{200}$ as a function of halo mass $M_{200}$ at the scale radii $r/r_{200} = 0.1$, 0.5, and 1.0 in non-radiative clusters simulated with the SPH code GADGET. Squares show entropy at $r_{200}$, triangles show entropy at $0.5r_{200}$, and diamonds show entropy at $0.1r_{200}$. Solid lines give the median values of $K/K_{200}$ at each radius, and dashed lines give the corresponding values from the power-law relation shown in Figure 1. No systematic trends with mass are evident.

clusters, which were extracted from a much larger simulation volume and then individually resimulated at a spatial resolution comparable to that of the $60\,h^{-1}\,M_{\odot}$ simulation, range from $5.5 \times 10^{14}\,h^{-1}\,M_{\odot}$ to $8.4 \times 10^{14}\,h^{-1}\,M_{\odot}$. Thus, all forty clusters in this overall sample are reasonably well-resolved.

Figure 1 shows the dimensionless entropy profiles of these clusters, averaged over radial bins. The average entropy in each spherical shell is defined to be the mean temperature in that shell divided by the two-thirds power of the mean electron density within the shell. Most of the spherically-averaged profiles are virtually identical at $r > 0.1r_{200}$, consistent with the expectation of self-similarity. Within the range $0.2 \stackrel{<}{\sim} r/r_{200} \stackrel{<}{\sim} 1.0$, the power law $K(r) \propto r^{1.1}$ shown by the dashed line is a good approximation, in agreement with the spherical-accretion models of Tozzi & Norman (2001) and Voit et al. (2003) and the simulations of Borgani et al. (2002). Inside of $0.1r_{200}$ there is more diversity. Some of the simulated clusters have nearly isentropic cores, while others do not. The flattening of the entropy profiles within the core is likely to be a real effect because the degree of flattening does not depend on cluster mass. If the flattening were due to a resolution effect, then it would be more pronounced in smaller, lower-mass clusters, whose physical size is smaller relative to the resolution length of the simulation. However, the same kind of flattening is seen in the better-resolved, higher-mass clusters simulated by Kay et al. (2004).

Figure 2 shows that dimensionless entropy measured at

a fixed scale radius does not depend on halo mass. No significant deviations from the approximate self-similar profile $K(r) = 1.32\,K_{200}\,(r/r_{200})^{1.1}$ are seen over the entire mass range, from $2 \times 10^{13}\,h^{-1}\,M_{\odot}$ to $8 \times 10^{14}\,h^{-1}\,M_{\odot}$. We have assessed the scatter in dimensionless entropy with the quantity

$$\frac{\Delta K}{K} \equiv \frac{K_{90\%} - K_{10\%}}{2K_{50\%}} \quad , \tag{4}$$

where $K_{X\%}$ is the $X$th percentile of the dimensionless entropy at a given radius. The average value of $\Delta K/K$ in the range $0.2 < r/r_{200} < 1.0$ is 0.12, and over the larger range $0.02 < r/r_{200} < 1.8$ its value is 0.28.

### 2.3 AMR Simulations

The other set of clusters we will consider was produced by the adaptive-mesh refinement code ENZO (Bryan 1999; Norman & Bryan 1999; O'Shea et al. 2004) with $\Omega_M = 0.3$, $\Omega_\Lambda = 0.7$, $\Omega_b = 0.04$, $h = 0.67$, and $\sigma_8 = 0.9$. Twenty-one of these non-radiative clusters were modeled within a box of comoving length $50\,h^{-1}$ Mpc using mesh refinement to produce an effective resolution of $20\,h^{-1}$ kpc in comoving coordinates. Further details about this simulation are given in Bryan & Voit (2001). To populate the upper end of the mass range, we added ten more clusters to our sample, drawn from the simulation described in Loken et al. (2002), with a box size of $256\,h^{-1}$ Mpc and an effective resolution of $15\,h^{-1}$ kpc. That larger simulation assumed a slightly different cosmology, with $\Omega_M = 0.3$, $\Omega_\Lambda = 0.7$, $\Omega_b = 0.026$, $h = 0.7$, and $\sigma_8 = 0.928$. However, dividing by the appropriate value of $K_{200}$ when constructing the dimensionless entropy profiles compensates for the differing baryon density scale. The overall AMR cluster set ranges in mass from $2.7 \times 10^{13}\,h^{-1}\,M_{\odot}$ to $1.4 \times 10^{15}\,h^{-1}\,M_{\odot}$.

As can be seen in Figure 3, the entropy profiles measured in this sample of simulated clusters are also nearly self-similar. Beyond the scale radius $0.2r_{200}$, the power-law slope and normalization of the dimensionless entropy profiles is quite close to those found in the SPH clusters, as illlustrated by the dashed line. However, the AMR profiles within this radius are significantly flatter than the SPH profiles (§ 3.1).

Likewise, the dimensionless entropy profiles of our AMR clusters also show no systematic trends with mass. Figure 4 samples the dimensionless entropy in this set of clusters at the same three scale radii as in Figure 2. Again, the points cluster around the median profile, with no dependence on $M_{200}$. The scatter in entropy likewise has properties similar to those found in the SPH simulation: $\Delta K/K = 0.21$ over the range $0.2 \stackrel{<}{\sim} r/r_{200} \stackrel{<}{\sim} 1.0$ and $\Delta K/K = 0.31$ over the complete range.

### 3 CROSS-COMPARISON OF SIMULATIONS

It should already be clear from the preceding section that the median dimensionless entropy profiles found in both cluster simulations are nearly the same outside of $0.2r_{200}$. Here we discuss some of the systematic differences between the two sets of simulated clusters and then provide a simple analytical formula for the median entropy profile that is consistent with
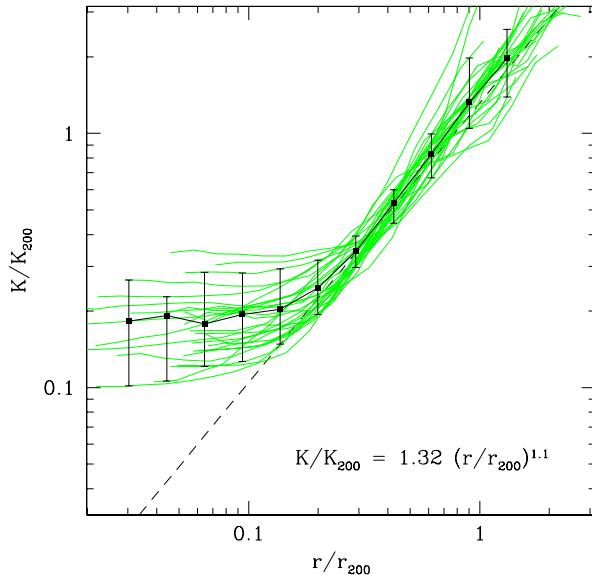
**Figure 3.** Dimensionless entropy $K/K_{200}$ as a function of scale radius $r/r_{200}$ for 31 clusters simulated with the AMR code ENZO. As in Figure 1, most of the entropy profiles shown lie close to the relation $K/K_{200} = 1.32(r/r_{200})^{1.1}$ in the radial range $0.2 \lesssim r/r_{200} \lesssim 1.0$. However, the flattening at smaller radii is more pronounced than in the SPH simulation, leading to substantially higher entropy levels near the origin.
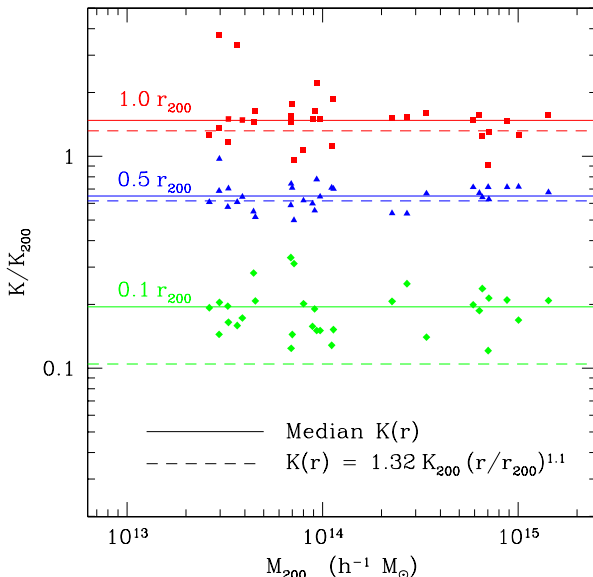


**Figure 4.** Dimensionless entropy $K/K_{200}$ as a function of halo mass $M_{200}$ at the scale radii $r/r_{200} = 0.1$, 0.5, and 1.0 in non-radiative clusters simulated with the AMR code ENZO. Squares show entropy at $r_{200}$, triangles show entropy at $0.5r_{200}$, and diamonds show entropy at $0.1r_{200}$. Solid lines give the median values of $K/K_{200}$ at each radius, and dashed lines give the corresponding values from the power-law relation shown in Figure 1. As in Figure 2, there are no discernible systematic trends with mass.

with both samples. To help observers use this formula, we conclude this section with a brief comparison to actual data, including a discussion of how offsets of $T_X$ with respect to $T_{200}$ affect the determination of the baseline profile for an observed cluster.

### 3.1 Entropy within the Core

The median dimensionless entropy profiles of clusters in our two simulation sets agree well outside the cluster core but disagree within the cluster core. Figure 5 illustrates the discrepancy. This type of discrepancy between SPH and AMR is nothing new. It was previously hinted at in the Santa Barbara cluster comparison (Frenk et al. 1999), but that result was not definitive because the sample size was a single cluster. Here we confirm it for a large sample of clusters with a range of masses and simulated with substantially higher spatial and mass resolution. Thus, we do not attempt to fit an analytical form to our median profiles within $0.1r_{200}$; the numerical techniques used to model this region do not yet give a reliable answer.

Because the primary purpose of this paper is to provide a baseline profile for observers to use outside the cluster core, we leave a detailed analysis of the reasons for this entropy discrepancy for future work. It is an important problem to pursue because of its implications for cooling and condensation of gas within cluster cores. Larger amounts of entropy production within the core, as in the AMR code, will more effectively inhibit cooling there, perhaps mitigating the "cooling-flow problem" in clusters of galaxies (see Donahue & Voit 2004, for a recent review).

### 3.2 Power-Law Approximations

Previous theoretical work has shown that the entropy profiles of non-radiative clusters approximately follow a power law with $K(r) \propto r^{1.1}$ (e.g., Tozzi & Norman 2001; Borgani et al. 2002; Voit et al. 2003), but these efforts have not provided a normalization for that power-law profile in a form that is useful to observers. Here we rectify that situation. If we fix the power-law slope of the entropy profile at 1.1 and fit the SPH clusters in the radial range $0.2 \leqslant r/r_{200} \leqslant 1.0$, we find

$$K(r) = 1.32 \pm 0.03 \, K_{200} \, (r/r_{200})^{1.1} \ . \qquad (5)$$

Doing the same for the AMR clusters yields

$$K(r) = 1.41 \pm 0.03 \, K_{200} \, (r/r_{200})^{1.1} \ , \qquad (6)$$

a normalization just slightly higher than that for the SPH clusters.

Figure 5 compares the power-law fit from equation (5) with the median profiles from both simulations and with two other analytical entropy profiles. One of the analytical profiles is constructed from the analytical temperature and density profiles developed by Rasia et al. (2004) to fit their SPH models of non-radiative clusters. The other is the entropy profile of intracluster gas with an NFW density distribution with concentration $c = 5$ assuming that it is in hydrostatic equilibrium within a dark-matter halo whose density distribution has the same shape (Voit & Bryan 2001; Voit et al. 2002). All of these profiles agree very well with the power-law profile of equation (5) in the range $0.2 \leqslant r/r_{200} \leqslant 1.0$.
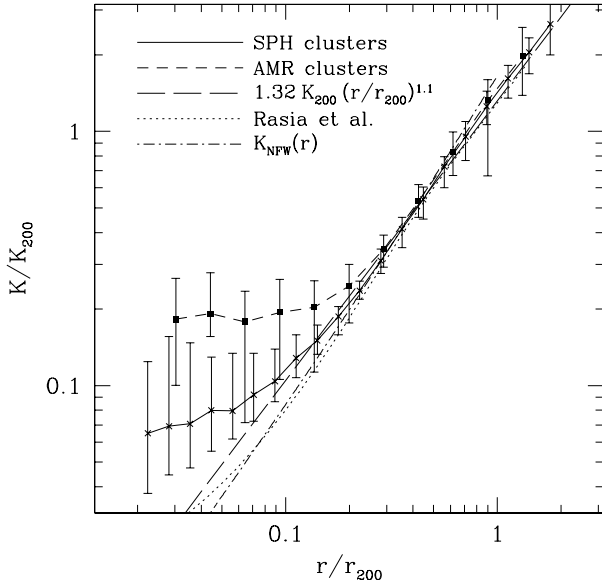
**Figure 5.** Median entropy profiles from cluster simulations without cooling or non-gravitational heating. A solid line connecting crosses shows the median profile for the SPH clusters. A dashed line connecting squares shows the median profile for the AMR clusters. Error bars give the 10% percentile to 90% percentile range. The long dashed line illustrates the power-law approximation $K(r) = 1.32\,K_{200}\,(r/r_{200})^{1.1}$. The dotted line gives an analytical entropy profile derived from simulations by Rasia et al. (2004). The dot-dashed line shows the profile $K_{\rm NFW}(r)$ corresponding to an NFW gas-density profile of concentration $c = 5$ that is in hydrostatic equilibrium within a dark-matter density profile of identical shape (Voit et al. 2002). Notice that both of the median profiles agree very well in the range $0.2 < r/r_{200} < 1.0$ and that the analytical approximations accurately represent the median profiles in this range. However, the AMR and SPH median profiles differ by as much as a factor of two within the cluster core.

Also, the power-law profile remains a good representation of our SPH simulations down to $\approx 0.1\,r_{200}$. We note, however, that the Rasia et al. (2004) profile shows much less flattening in the core than the simulations analyzed in this paper, perhaps because it is based on an earlier version of GADGET that does not explicitly conserve entropy (see also Ascasibar et al. 2003).

Up to this point, we have been fitting the median profiles with a $K(r) \propto r^{1.1}$ power law because that is the standard power-law index in the literature, and it appears to be consistent with the highest quality cluster observations (e.g., Pratt & Arnaud 2003). However, Figure 6 suggests that a power-law index of 1.1 might be slightly too shallow to be the best representation of the median profiles outside of $0.2r_{200}$. Fitting a power-law of index 1.2 to the median profiles gives the following results:

$$K(r) = 1.43 \pm 0.01\,K_{200}\,(r/r_{200})^{1.2} \quad . \tag{7}$$

for the SPH clusters and

$$K(r) = 1.48 \pm 0.02\,K_{200}\,(r/r_{200})^{1.2} \tag{8}$$

for the AMR clusters. Figure 7 shows that dividing the median profiles by equation (7) makes the resulting profiles flatter, indicating that $K(r) \propto r^{1.2}$ is a better description
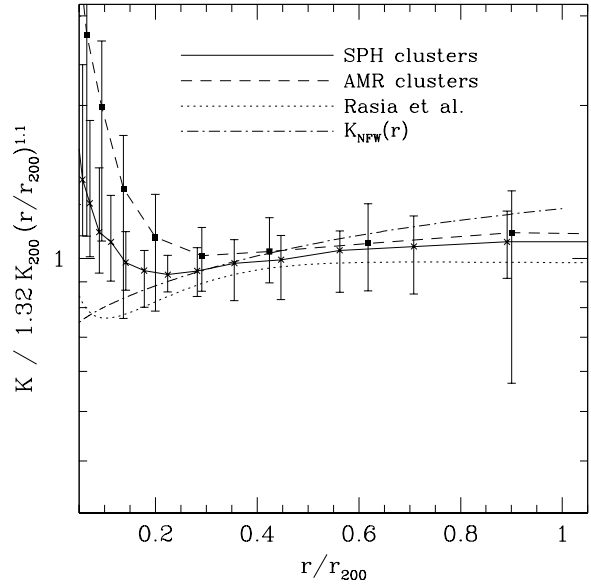
**Figure 6.** Median dimensionless entropy profiles from simulations, divided by the power-law profile $K(r) = 1.32\,K_{200}\,(r/r_{200})^{1.1}$. Crosses connected by a solid line show the median profile from the SPH simulation, and squares connected by a dashed line show the median profile from the AMR simulation. Dashed and dot-dashed lines show the Rasia et al. (2004) and NFW-like profiles, respectively. A slight rise in the median points as radius increases beyond $0.2r_{200}$ suggests that the assumed power-law index of 1.1 is slightly too small.

of the outer parts of non-radiative clusters. Indeed, if we allow the power-law index to be a free parameter and fit the median profiles in the range $0.2 \leqslant r/r_{200} \leqslant 1.0$, we find

$$K(r) = 1.45 \pm 0.01\,K_{200}\,(r/r_{200})^{1.21 \pm 0.01} \quad . \tag{9}$$

for the SPH clusters and

$$K(r) = 1.51 \pm 0.03\,K_{200}\,(r/r_{200})^{1.24 \pm 0.03} \tag{10}$$

for the AMR clusters. In all of these fits the error bars correspond to $1\sigma$.

### 3.3 Applications of the Baseline Profiles

The entropy profiles computed here for non-radiative clusters provide a baseline for assessing the impact of non-gravitational processes on the intracluster medium. However, in order to compare the entropy profiles of a real cluster to these self-similar baselines, one needs to know the value of $K_{200}$ for the cluster. This characteristic entropy scale can be simply computed from equations (1) and (2) if the cluster mass $M_{200}$ has been accurately measured. Otherwise, one must infer $K_{200}$ from $T_{\rm X}$ and a relation between $T_{200}$ and $T_{\rm X}$ or, equivalently, a relation between $M_{200}$ and $T_{\rm X}$. Figure 8 compares entropy values measured at $0.1r_{200}$ with those predicted for self-similar clusters. The long-dashed and dotted lines show the predictions for non-radiative AMR and SPH clusters, respectively. Here we set $T_{\rm X} = T_{200}$ because any offset between $T_{\rm X}$ and $T_{200}$ is small compared with the difference between the two simulation sets. As shown by Ponman et al. (2003) and Voit & Ponman (2003), the measurements clearly do not agree with the self-similar models,
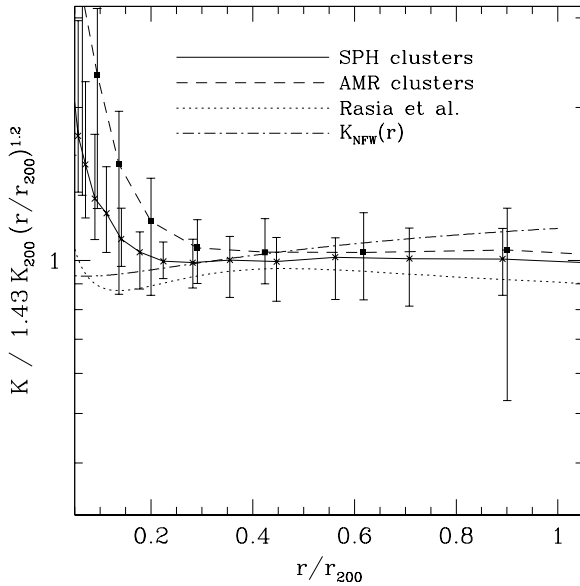
**Figure 7.** Median dimensionless entropy profiles from simulations, divided by the power-law profile $K(r) = 1.43\,K_{200}\,(r/r_{200})^{1.2}$. Crosses connected by a solid line show the median profile from the SPH simulation, and squares connected by a dashed line show the median profile from the AMR simulation. Dashed and dot-dashed lines show the Rasia et al. (2004) and NFW-like profiles, respectively. A power-law index of 1.2 seems to be a better description of the entropy profile beyond $0.2r_{200}$ than the standard index of 1.1.
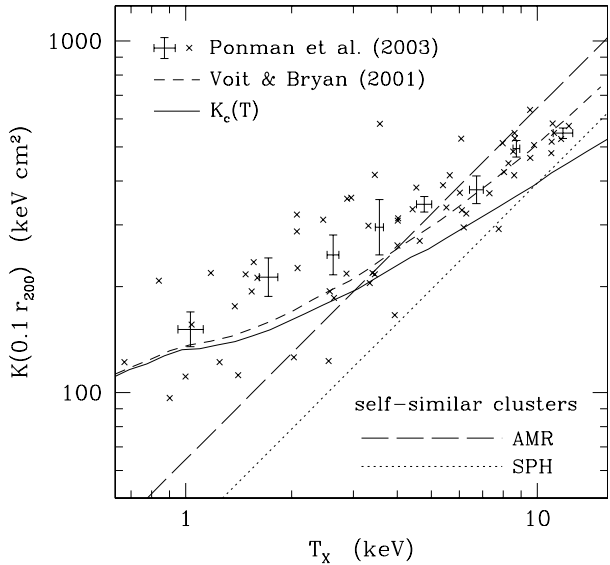


**Figure 8.** Relationship between core entropy and the cooling threshold. Each point with error bars shows the mean core entropy $K_{0.1}$, measured at $0.1\,r_{200}$, for eight clusters within a given temperature bin, and small crosses show measurements for individual clusters (Ponman et al. 2003). The long-dashed and dotted lines show self-similar relations calibrated using the median values of $K_{0.1}$ derived from our AMR and SPH simulations, respectively, assuming that $T_{\mathrm{X}} = T_{200}$. High-temperature clusters appear to be consistent with the median self-similar profiles, but the trend to lower-temperatures more closely tracks the cooling threshold $K_c(T)$ (solid line), defined to be the entropy at which the cooling time equals 14 Gyr (Voit & Ponman 2003). The short-dashed line shows the predicted entropy at $0.1r_{200}$ in the model of Voit & Bryan (2001).

which predict that $K(0.1r_{200}) \propto T_{\mathrm{X}}$. Instead, the measurements track the cooling threshold $K_c(T) \propto T_{\mathrm{X}}^{2/3}$. We wish to point out, however, that the hot clusters are consistent with non-radiative models at this radius. This finding contrasts with Figure 1 of Voit & Ponman (2003), in which the locus for self-similar clusters is mistakenly a factor of two too low, owing to a unit conversion error.

Figure 9 compares entropy values measured at $r_{500} \approx 0.66r_{200}$, within which the mean mass density is 500 times the critical density, with the baseline profiles. The solid line shows the baseline entropy level derived assuming $T_{\mathrm{X}} = T_{200}$, which slightly exceeds the measured entropy levels at this radius in hot clusters. This apparent shortfall in the observed entropy levels of hot clusters goes away when we account for the difference between $T_{\mathrm{X}}$ and $T_{200}$. A dashed line shows the baseline entropy level at $r_{500}$ computed using values of $K_{200}$ derived from the $M_{200}$-$T_{\mathrm{X}}$ relation of Sanderson et al. (2003), and this line is consistent with the entropy measurements at $r_{500}$ in hot clusters. This consistency again contrasts with the results of Voit & Ponman (2003), in which the locus for self-similar clusters was mistakenly placed too low. However, clusters below about 6 keV still show a clear entropy excess, which is even more pronounced when the observed $M_{200}$-$T_{\mathrm{X}}$ relation is used to compute $K_{200}$.

## 4 SUMMARY

Our intention in this paper has been to provide a simple analytical form for the entropy profiles of non-radiative clusters

to use as a baseline when trying to measure the impact of non-gravitational processes on the intracluster medium. To that end, we analyzed two different sets of simulated clusters, one created with a Lagrangian SPH code and the other with an Eulerian AMR code. Thirty to forty entropy profiles were produced by each code and these profiles were found to be approximately self-similar, with the $K(r/r_{200}) \propto T_{\mathrm{X}}$ scaling expected of non-radiative clusters. The simulated profiles depend very little on halo mass once the expected scaling is divided out. This result confirms that non-gravitational processes are necessary to produce the observed scaling relations of clusters.

The median entropy profiles from the two simulations agree to within 7% outside of $0.2r_{200}$ but disagree in the cluster core. In the outer parts of clusters the power-law profile $K(r) = 1.32\,K_{200}\,(r/r_{200})^{1.1}$ is a good representation of the baseline profile expected in the non-radiative case. However, our results suggest that the baseline profile in the radial range $0.2 \leqslant r/r_{200} \leqslant 1.0$ is better fit by a $K(r) \propto r^{1.2}$ power law, rather than the standard $K(r) \propto r^{1.1}$ law found by Tozzi & Norman (2001). Inside of $0.2r_{200}$ the discrepancy between the AMR clusters and the SPH clusters is quite substantial. Tracking down the origin of this discrepancy is important, because radiative cooling rates in clusters depend on the core entropy level.

Our comparison between the self-similar entropy profiles derived from these simulated clusters with measure-
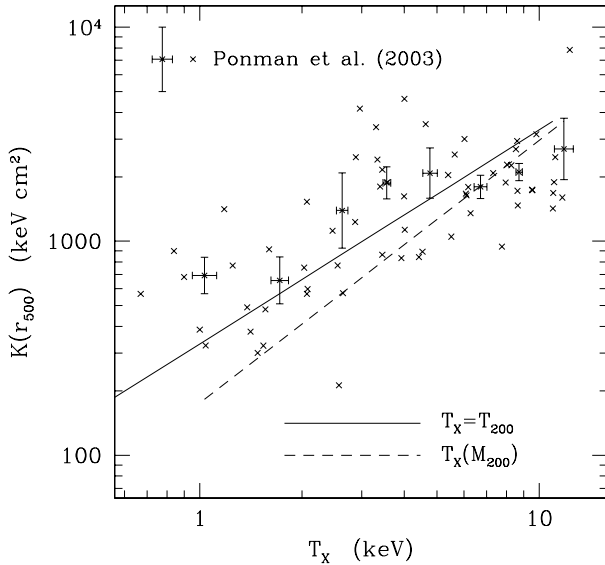
**Figure 9.** Entropy at $r_{500}$ as a function of cluster temperature. Each point with error bars shows the mean value of $K(r_{500})$ implied by the density and temperature profiles of eight clusters within that temperature bin (Ponman et al. 2003), and small crosses show measurements for individual clusters. The solid line shows the median entropy at $r_{500}$ for self-similar clusters, assuming that $T_X = T_{200}$. The dashed line shows how the mapping of this median entropy onto $T_X$ changes when the $T_X(M_{200})$ relationship observed by Sanderson et al. (2003) is used to determine $T_X$. The most massive clusters are consistent with the self-similar clusters modeled without non-gravitational processes when this observational $M_{200}$-$T_X$ relation is used.

ments of entropy at $0.1\,r_{200}$ and $r_{500}$ in real clusters updates and corrects the findings of Voit & Ponman (2003). There is a clear entropy excess in cool clusters, presumably stemming from non-gravitational processes. However, clusters hotter than $\sim 6\,\mathrm{keV}$ appear to converge to the self-similar profile at radii $\gtrsim 0.1\,r_{200}$.

**REFERENCES**

Allen, S. W., & Fabian, A. C. 1998, MNRAS, 297, L57
Arnaud, M., & Evrard, A. E. 1999, MNRAS, 305, 631
Ascasibar, Y., Yepes, G., Müller, V., & Gottlöber, S. 2003, MNRAS, 346, 731
Balogh, M. L., Pearce, F. R., Bower, R. G., & Kay, S. T. 2001, MNRAS, 326, 1228

Borgani, S., Governato, F., Wadsley, J., Menci, N., Tozzi, P., Quinn, T., Stadel, J., & Lake, G. 2002, MNRAS, 336, 409
Borgani, S., Finoguenov, A., Kay, S.T., Ponman, T.J., Springel, V., Tozzi, P., & Voit, G.M. 2005, MNRAS, in press, astro-ph/0504265
Bryan, G. L. 1999, Computing in Science and Engineering, 1, 46
Bryan, G. L., & Voit, G. M. 2001, ApJ, 556, 590
David, L. P., Jones, C., & Forman, W. 1995, ApJ, 445, 578
Donahue, M., & Voit, G. M. 2004, in Carnegie Astrophysics Series, Vol. 3: Clusters of Galaxies: Probes of Cosmological Structure and Galaxy Evolution, ed. J. S. Mulchaey, A. Dressler, & A. Oemler, in press
Edge, A. C., & Stewart, G. C. 1991, MNRAS, 252, 414
Eke, V. R., Navarro, J. F., & Frenk, C. S. 1998, ApJ, 503, 569
Evrard, A. E., & Henry, J. P. 1991, ApJ, 383, 95
Frenk, C. S., et al. 1999, ApJ, 525, 554
Kaiser, N. 1986, MNRAS, 222, 323
—. 1991, ApJ, 383, 104
Kay, S. T. 2004, MNRAS, 347, L13
Kay, S. T., Thomas, P. A., Jenkins, A., & Pearce, F. R. 2004, MNRAS, 355, 1091
Kay, S. T., Thomas, P. A., & Theuns, T. 2003, MNRAS, 343, 608
Loken, C., Norman, M. L., Nelson, E., Burns, J., Bryan, G. L., & Motl, P. 2002, ApJ, 579, 571
Markevitch, M. 1998, ApJ, 504, 27
Muanwong, O., Thomas, P. A., Kay, S. T., Pearce, F. R., & Couchman, H. M. P. 2001, ApJ, 552, L27
Navarro, J. F., Frenk, C. S., & White, S. D. M. 1995, MNRAS, 275, 720
Norman, M. L., & Bryan, G. L. 1999, in ASSL Vol. 240: Numerical Astrophysics, 19–+
O'Shea, B. W., et al. 2004, astro-ph/0403044
Ponman, T. J., Sanderson, A. J. R., & Finoguenov, A. 2003, MNRAS, 343, 331
Pratt, G. W., & Arnaud, M. 2003, A&A, 408, 1
Pratt, G. W., & Arnaud, M. 2005, A&A, 429, 791
Rasia, E., Tormen, G., & Moscardini, L. 2004, MNRAS, 351, 237
Sanderson, A. J. R., Ponman, T. J., Finoguenov, A., Lloyd-Davies, E. J., & Markevitch, M. 2003, MNRAS, 340, 989
Springel, V., & Hernquist, L. 2002, MNRAS, 333, 649
Springel, V., Yoshida, N., & White, S. D. M. 2001, New Astronomy, 6, 79
Tornatore, L., Borgani, S., Springel, V., Matteucci, F., Menci, N., & Murante, G. 2003, MNRAS, 342, 1025
Tozzi, P., & Norman, C. 2001, ApJ, 546, 63
Valageas, P., Schaeffer, R., & Silk, J. 2003, MNRAS, 344, 53
Valdarnini, R. 2003, MNRAS, 339, 1117
Voit, G. M. 2005, Rev. Mod. Phys., 77, 207
Voit, G. M., Balogh, M. L., Bower, R. G., Lacey, C. G., & Bryan, G. L. 2003, ApJ, 593, 272
Voit, G. M., & Bryan, G. L. 2001, Nature, 414, 425
Voit, G. M., Bryan, G. L., Balogh, M. L., & Bower, R. G. 2002, ApJ, 576, 601
Voit, G. M., & Ponman, T. J. 2003, ApJ, 594, L75
White, S. D. M., & Frenk, C. S. 1991, ApJ, 379, 52